COMPARATIVE MAGNETIC AND PHOTOCATALYTIC PROPERTIES OF COPRECIPITATED ZINC FERRITE NANOPARTICLES BEFORE AND AFTER CALCINATION

S. A. Seyyed Ebrahim[1*], M. Ebrahimi[1] and S. M. Masoudpanah[2]

* *saseyyed@ut.ac.ir*

Received: September 2016 **Accepted: February 2017**

[1] Advanced Magnetic Materials Research Center, School of Metallurgy and Materials, College of Engineering, University of Tehran, Tehran, Iran.

[2] School of Metallurgy & Materials Engineering, Iran University of Science and Technology, Tehran, Iran.

Abstract: *In this work, the effects of co-precipitation temperature and post calcination on the magnetic properties and photocatalytic activities of $ZnFe_2O_4$ nanoparticles were investigated. The structure, magnetic and optical properties of zinc ferrite nanoparticles were characterized by X-ray diffraction (XRD), vibrating sample magnetometry and UV–Vis spectrophotometry techniques. The XRD results showed that the coprecipitated as well as calcined nanoparticles are single phase with partially inverse spinel structures. The magnetization and band gap decreased with the increasing of co-precipitation temperature through the increasing of the crystallite size. However, the post calcination at 500°C was more effective on the decreasing of magnetization and band gap. Furthermore, photocatalytic activity of zinc ferrite nanoparticles was studied by the degradation of methyl orange under UV-light irradiation. Compare with the coprecipitated $ZnFe_2O_4$ nanoparticles with 5% degradation of methyl orange after 5 h UV-light light radiation, the calcined $ZnFe_2O_4$ nanoparticles exhibited a better photocatalytic activity with 20% degradation.*

Keywords: *Zinc ferrite, Co-precipitation, Band gap, Photocatalytic activity*

1. INTRODUCTION

Zinc ferrite semiconductor photocatalyst has been applied widely to degrade the organic pollutants for the remediation of hazardous wastes, contaminated groundwater and the control of toxic air contaminants [1]. Zinc ferrite with spinel crystal structure offers the advantage of a narrow band gap (1.9 eV) capable of absorbing visible light, as well as the spinel crystal structure, which enhanced efficiency due to the more available catalytic sites by virtue of the crystal lattice [2]. Moreover, the used magnetic $ZnFe_2O_4$ powders are easy to collect, which make $ZnFe_2O_4$ powders one of the most promising photocatalysts in the field of industrial photodegradation of organic pollutants [3]. However, the photocatalytic activity of pure $ZnFe_2O_4$ is worse than that of anatase TiO_2, due to the poor separation efficiency of photogenerated electrons and holes [4]. Consequently, many strategies, including the surface modification [5], surface area [6], metal ion (e.g. Ag) doping [7], nonmetal ion (e. g. S) doping [8], coupling with other semiconductors [9–11], etc. have been adopted to synthesize $ZnFe_2O_4$-based photocatalysts. Furthermore, several synthesis methods such as ball milling [12], sol-gel [13], co-precipitation [14], hydrothermal [15] auto-combustion [16] and ultrasonic cavitation [17] have been used to promote the charge-transfer process and increase the surface/volume ratio, and finally promote the photocatalytic activity of $ZnFe_2O_4$. Fan et al. [15] reported the various special $ZnFe_2O_4$ nanoparticles synthesized via the different hydrothermal processes exhibited the better photocatalytic activities compare to the bulk $ZnFe_2O_4$ samples, due to the high surface area structures [18]. However, the co-precipitation is a simple technique to synthesize the ferrite nanoparticles at low temperatures. Furthermore, the coprecipitated nanoparticles with high purity and no agglomeration are appropriate for photocatalytic activity [19].

In this work, we have synthesized zinc ferrite nanoparticles via co-precipitation technique and investigated the effects of the co-precipitation temperature and post calcination process on the magnetic properties and the photocatalytic

[Downloaded from herasat.iust.ac.ir on 2025-07-19]

[DOI: 10.22068/ijmse.14.1.5]

activities under UV light radiation.

2. EXPERIMENTAL PROCEDURE

Iron (III) chloride hexahydrate ($FeCl3.6H_2O$), zinc (II) chloride ($ZnCl_2$), sodium hydroxide (NaOH) and acetone with analytical grade were purchased from Merck Co.

Zinc ferrite nanoparticles were synthesized by chemical co-precipitation method. In this procedure, a mixed aqueous solution prepared by dissolving iron and zinc chlorides with the molar ratio of Fe to Zn as 2:1 in 100 mL distilled water. 50 mL aqueous solution of 1.5 M NaOH was used as the precipitating agent. Metal chloride and NaOH solutions were added drop wise from two separate burettes into a reaction vessel containing 100 mL of distilled water for obtaining uniform particle size distribution. The reaction vessel was heated up to the desired temperature (40-80 °C) under magnetic stirring. The resultant precipitations were collected and centrifuged at 6000 rpm and then washed with distilled water and acetone for several times and finally dried in air. Some of the coprecipitated $ZnFe_2O_4$ nanoparticles were also calcined at 500°C for 1 h.

The phase composition was analyzed by Philips X'pert Pro prefix powder X-ray diffractometer using monochromatic CuKα radiation (λ = 1.5405 Å). The average crystallite size of the samples was also calculated by using peak broadening of (311) peak in Scherrer's equation.

The morphology and microstructure were observed by a Philips CM200 transmission electron microscope (TEM) at 200 kV. Selected area electron diffraction (SAED) pattern was also taken on TEM. A vibrating sample magnetometer (Meghnatis Daghigh Kavir Co., Iran) was employed to measure magnetic properties of the samples at room temperature.

The optical absorption spectrum was recorded on an Avaspec 2048 TEC UV–Vis spectrophotometer with the wavelength range of 300–800 nm. Photocatalytic activity of the prepared $ZnFe_2O_4$ was evaluated by the degradation of methyl orange in aqueous solution under UV light irradiation. A cut-off filter was placed under the UV lamp (8 W) to remove all wavelengths less than 400 nm. In each experiment, 0.1 g of photocatalyst was added into 100 ml methyl orange solution with a concentration of 10 mg/l. The suspension was magnetically stirred in the darkness for 1 h to establish the adsorption/desorption equilibrium at room temperature, then the solution was irradiated using UV radiation. During irradiation, stirring was continued to keep the mixture in suspension. At regular intervals, samples were taken from the suspension and then centrifuged to remove the photocatalyst particles. The change in the concentration of each degraded solution was monitored on UV–Vis–NIR spectrophotometer Raylight UV-1600 via measuring the absorbance in 300–600 nm for methyl orange.

3. RESULTS AND DISCUSSION

Fig. 1 shows XRD patterns of the samples coprecipitated at different temperatures (40-80°C) and the sample coprecipitated at 80 °C and subsequently calcined at 500°C. The XRD results indicated that the all samples were single phase zinc ferrite and all peaks can be indexed to cubic spinel structure of $ZnFe_2O_4$ (JCPDS NO. 22-1012). However, the diffraction peaks became narrower and sharper with increasing precipitation temperature from 40°C to 80°C and calcination at 500°C, indicating an increase of crystallinity and crystallite size. Moreover, the measured lattice parameters decreased with increasing synthesis temperature, as presented in Table 1. Furthermore, the lattice parameter was larger than that of the normal spinel structure of zinc ferrite (a=8.4412 Å). This indicated that the samples had partially inverse structure, because of the substitution of some Zn^{2+} cations with large ionic radius (0.74 Å) for Fe^{3+} cations (0.65 Å) in octahedral sites which resulted in the expansion of the spinel lattice [20]. However, the redistribution of Zn^{2+} and Fe^{3+} cations into tetrahedral and octahedral sites, respectively, after calcination at 500 °C resulted in the smallest lattice parameter. The presence of (222) peak in Fig. 1d for the sample calcined at 500 °C also confirmed the decreasing of the inversity according to the literature [21].

[Downloaded from herasat.iust.ac.ir on 2025-07-19]

[DOI: 10.22068/ijmse.14.1.5]

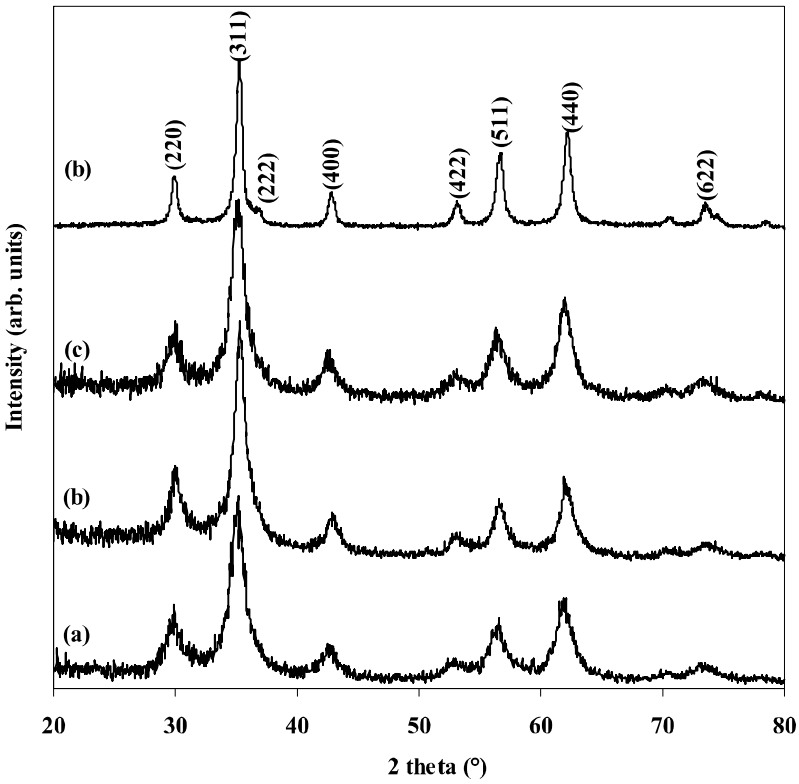

Fig. 1. XRD patterns of $ZnFe_2O_4$ nanoparticles synthesized at (a) 40 °C, (b) 60 °C and (c) 80 °C and (d) synthesized at 80 °C and post calcined at 500 °C..

TEM images of zinc ferrite nanoparticles, one only coprecipitated at 80°C and the other post calcined at 500 °C are presented in Fig. 2. It can be seen that the $ZnFe_2O_4$ nanoparticles are monodisperse and spherical. The average particle size of zinc ferrite nanoparticles precipitated at 80°C is 11 nm, increasing up to 21 nm after calcination at 500°C, which are in agreement with the crystallite sizes calculated from XRD patterns (Table 1).

The magnetization curves of the samples shown their XRD patterns in Fig. 1 are exhibited

Table 1. Lattice parameter, crystallite size, magnetization at 10 kOe and band gap as a function of synthesis temperature.

Temperature (°C)	a (Å)	Crystallite size (nm)	Magnetization (emu/g)	Eg (eV)
40	8.4480	7	7.2	2.05
60	8.4469	8	6.5	1.96
80	8.4439	10	5.4	1.83
500	8.4420	19	2.7	1.88

[Downloaded from herasat.iust.ac.ir on 2025-07-19]

[DOI: 10.22068/ijmse.14.1.5]

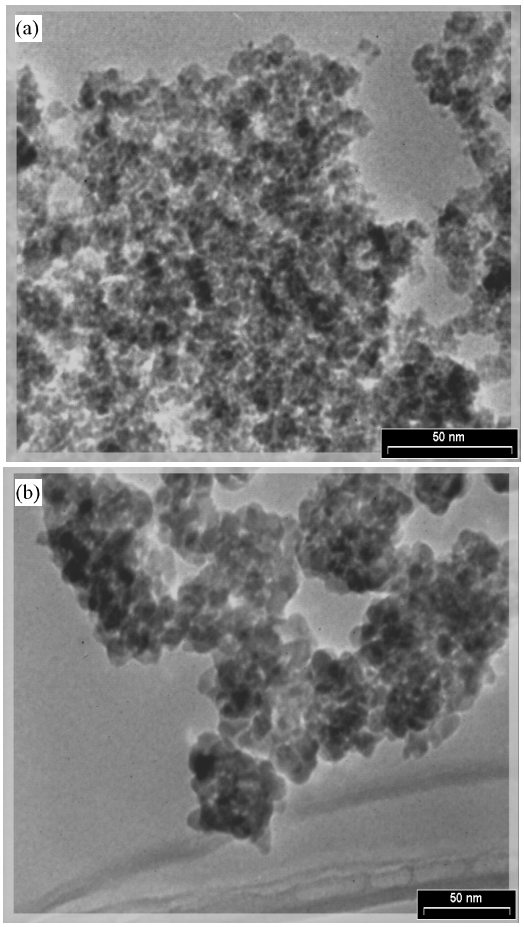

Fig. 2. TEM micrograph of $ZnFe_2O_4$ nanoparticles (a) synthesized at 80 °C and (b) synthesized at 80 °C and post calcined at 500 °C.

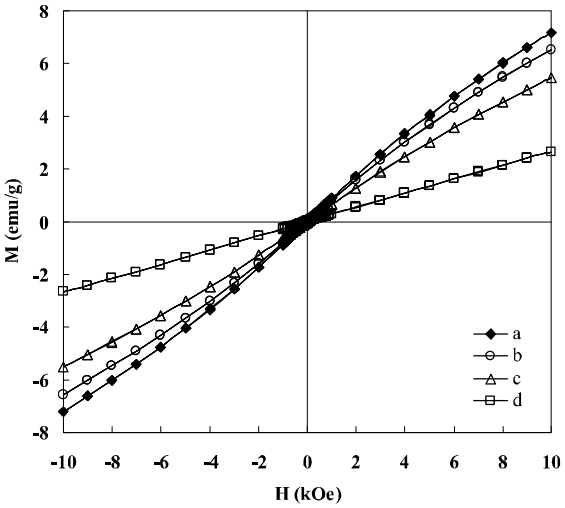

Fig. 3. Magnetization curves of $ZnFe_2O_4$ nanoparticles synthesized at (a) 40 °C, (b) 60 °C and (c) 80 °C and (d) synthesized at 80 °C and post calcined at 500 °C.

in Fig. 3. The magnetization curves of the samples were linear with zero coercivity indicating that the zinc ferrite nanoparticles were superparamagnetic. Although the bulk $ZnFe_2O_4$ with a normal spinel structure is paramagnetic, these zinc ferrite nanoparticles exhibited a ferrimagnetic behavior, due to the redistribution of iron and zinc cations into octahedral and tetrahedral sites [21, 22]. Furthermore, the samples were not fully saturated at 10 kOe, due to the presence of superparamagnetic and single domain particles [23]. The magnetizations at 10 kOe for these samples were also presented in Table 1. The magnetization decreased with increasing the co-precipitation temperature, due to the decreasing of inversity originated from the increasing of crystallite size [19] which is more obvious in the calcined sample.

The UV–vis absorption spectra of these samples are shown in Fig. 4 (top). The absorption spectra showed that the $ZnFe_2O_4$ nanoparticles absorbed considerable amounts of visible light, suggesting their potential applications as visible-light photocatalysts. The optical direct band gap, Eg, was determined from Fig. 4 (bottom) by the equation $(\alpha h\nu)^2=A(h\nu-E_g)$, where $h\nu$ is the photon energy in eV, α is the absorption coefficient, and A is a constant relative to the material [24]. The band gap of the samples was also given in Table 1. The absorption of $ZnFe_2O_4$ in the visible region can be attributed to the photoexcited electron transition from O_{2p} level into Fe_{3d} level since the energy band structure of $ZnFe_2O_4$ is generally defined by considering the O_{2p} level as the valence band and the Fe_{3d} level as the conduction band [25, 26]. Furthermore, the band gap energy decreased with increasing the crystallite size, due to the quantum-size effect [27].

The photocatalytic activities of the $ZnFe_2O_4$ samples, one only coprecipitated at 80°C and the other post calcined at 500°C, were investigated

[Downloaded from herasat.iust.ac.ir on 2025-07-19]

[DOI: 10.22068/ijmse.14.1.5]

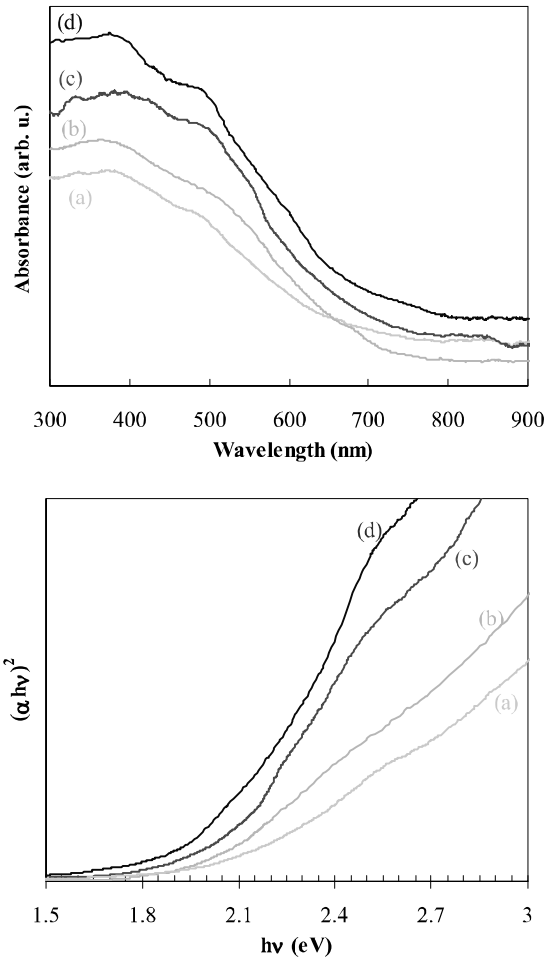

Fig. 4. UV–vis absorption spectra (top) and Tauc's plots ((αhν)2 vs. hν) (bottom) of $ZnFe_2O_4$ nanoparticles synthesized at (a) 40 °C, (b) 60 °C and (c) 80 °C and (d) synthesized at 80 °C and post calcined at 500 °C.

and the results were illustrated in Fig. 5. This figure shows that the dye concentration decreased just after removal of darkness, due to the partial adsorption of organic molecules on the surface of catalyst in the darkness. The coprecipitated $ZnFe_2O_4$ nanoparticles exhibited more reduction than that of the calcined sample, due to the lower crystallite size and higher specific surface areas [6]. With increasing the irradiation time, the relative concentration of dye decreased in the calcined sample to 80 % after 5 h, due to photocatalytic degradation of methyl orange. However, in the coprecipitated sample the

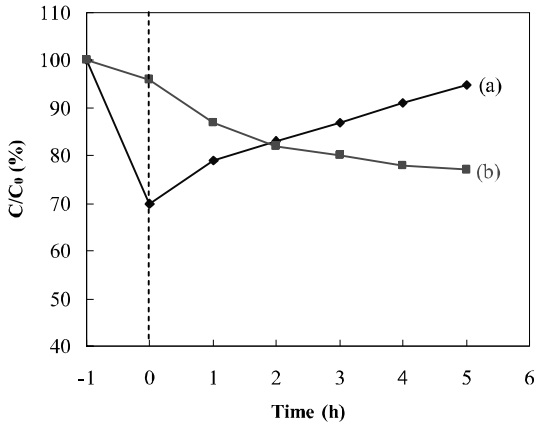

Fig. 5. Photodegradation of MO under UV light irradiation by $ZnFe_2O_4$ nanoparticles (a) synthesized at 80 °C and (b) synthesized at 80 °C and post calcined at 500 °C.

relative concentration increased in spite of more irradiation, because the absorbed organic molecules were released from the nanoparticle surface during the stirring, probably showing that 1 h stirring in darkness was not enough for equilibrium of absorption/desorption. In this sample, only 5 % of the dye degraded after 5 h light irradiation, due to the photocatalytic activity. Furthermore, the rather high photocatalytic activity of the calcined $ZnFe_2O_4$ nanoparticles can be attributed to the low band gap (1.88 eV). The lower band gap results in generation of more electrons and holes which interact with surface bound H_2O or OH^- to produce OH free radicals for the photocatalyticdegradation process.

4. CONCLUSIONS

Single phase zinc ferrite nanoparticles with partially inverse spinel structures have been synthesized by co-precipitation at various temperatures (40- 80°C) and post calcination at 500°C. The magnetization and band gap decreased with the increasing co-precipitation temperature. The calcined $ZnFe_2O_4$ nanoparticles exhibited better photocatalytic activity with 20% degradation, compared with the coprecipitated $ZnFe_2O_4$ nanoparticles with 5% degradation of

[Downloaded from herasat.iust.ac.ir on 2025-07-19]

[DOI: 10.22068/ijmse.14.1.5]

methyl orange after 5 h UV-light light radiation

REFERENCES

1. Casbeer, E., Sharma, V. K., Li, X. Z., "Synthesis and photocatalytic activity of ferrites under visible light: A review", Separ.Purif. Tech., 2012, 87. 1-14.
2. Dom, R., Subasri, R., Radha, K., Bors, P. H., "Synthesis of solar active nanocrystalline ferrite, MFe2O4 (M: Ca, Zn, Mg) photocatalyst by microwave irradiation", Solid State Commun., 2011, 151, 470-473.
3. Fu, Y. S., Wang, X., "Magnetically separable $ZnFe_2O_4$–graphene catalyst and its high photocatalytic performance under visible light irradiation", Ind. Eng. Chem. Res., 2011, 50, 7210-7218.
4. Cheng, P., Li, W., Zhou, T. L., Jin, Y. P., Gu, M. Y., "Physical and photocatalytic properties of zinc ferrite doped titania under visible light irradiation", J.Photochem.Photobiol. C, 2004, 168, 97-101.
5. Li, X. Y., Hou, Y., Zhao, Q. D., Teng, W., Hu, X. J., Chen, G. H., "Capability of novel $ZnFe_2O_4$ nanotube arrays for simulated-sunlight induced degradation of 4-chlorophenol", Chemosphere, 2011, 82, 581-586.
6. Jadhav, S. D., Hankare, P. P., Patil, R. P., Sasikala, R., "Effect of sintering on photocatalytic degradation of methyl orange using zinc ferrite", Materials Letters, 2011, 65, 371-373.
7. Cao, X. B., Gu, L., Lan, X. M., Zhao, C., Yao, D., Sheng, W. J., "Spinel $ZnFe_2O_4$ nanoplates embedded with Ag clusters: preparation, characterization, and photocatalytic application, Mater". Chem. Phys., 2007, 106, 175-180.
8. Liu, L. J., Zhang, G. L., Wang, L., Huang, T., Qin, L., "Highly active S-modified $ZnFe_2O_4$ heterogeneous catalyst and its photo-fenton behavior under UV–visible irradiation", Ind. Eng. Chem. Res., 2011, 50, 7219-7227.
9. Li, X. Y., Hou, Y., Zhao, Q. D., Chen, G. H., "Synthesis and photo-induced charge transfer properties of $ZnFe_2O_4$–sensitized TiO_2 nanotube-array electrode", Langmuir, 2011, 27, 3113-3120.
10. Kong, L., Jiang, Z., Xiao, T., Lu, L., Jones, M. O., Edwards, P. P., "Exceptional visible-light-driven photocatalytic activity over BiOBr–$ZnFe_2O_4$ heterojunctions, Chem.Commun., 2011, 47, 5512-5514.
11. Liu, G. G., Zhang, X. Z., Xu, Y. J., Niu, X. S., Zheng, L. Q., Ding, X. J., "Effect of $ZnFe_2O_4$ doping on the photocatalytic activity of TiO_2", Chemosphere, 2004, 55, 1287-1291.
12. Yao, C., Zeng, Q., Goya, G., Torres, T., Liu, J., Wu, H., Ge, M., Zeng, Y., Wang, Y., Jiang, J., $ZnFe_2O_4$ Nanocrystals: Synthesis and Magnetic Properties,J. Phys. Chem. C, 2007, 111, 12274-12278.
13. Wang, L., Zhou, Q., Li, F., "Ionic disorder and Yaffet–Kittel angle in nanoparticles of $ZnFe_2O_4$ prepared by sol-gel method", Phys.Stat., solidi (b), 2004, 241, 377-382.
14. Kundu, A., Upadhyay, C., and Verma, H., "Magnetic properties of a partially inverted zinc ferrite synthesized by a new co-precipitation technique using urea", Phys. Letter. A, 2003, 311, 410-415.
15. Fan, G. L., Gu, Z. J., Yang, L., Li, F., "Nanocrystalline zinc ferrite photocatalysts formed using the colloid mill and hydrothermal technique", Chem. Eng. J., 2009, 155, 534-541.
16. Zhang, R., Huang, J., Zhao, J., Sun, Z., Wang, Y., "Sol–gel auto-combustion synthesis of zinc ferrite for moderate temperature desulfurization", Energy & Fuels, 2007, 21, 2682-2687.
17. Reddy, B. R., Sivasankar, T., Sivakumar, M., and Moholkar, V. S., "Physical facets of ultrasonic cavitational synthesis of zinc ferrite particles, Ultrason". Sonochem.,2010, 17, 416-426.
18. G. L. Fan, Z. J. Gu, L. Yang, F. Li, "Nanocrystalline zinc ferrite photocatalysts formed using the colloid mill and hydrothermal technique", Chem. Eng. J., 2009, 155, 534-541.
19. RaeisiShahraki, R., Ebrahimi, M., Seyyed Ebrahimi, S. A., Masoudpanah, S. M., "Structural characterization and magnetic properties of superparamagnetic zinc ferrite nanoparticles synthesized by the co-precipitation method", J.Magn.Magn.Mater., 2012, 324, 3762-3765.
20. R. D. Shannon, "Revised effective ionic radii and systematic studies of interatomic distances

[Downloaded from herasat.iust.ac.ir on 2025-07-19]

[DOI: 10.22068/ijmse.14.1.5]

in halides and chalcogenides", Acta. Cryst. A, 1976, 32, 751-767.

21. Chinnasamy, C., Narayanasamy, A., Ponpandian, N., Chattopadhyay, K., Guerault, H., and Greneche, J., "Ferrimagnetic ordering in"; nanostructured zinc ferrite, Scr. Mater., 2001, 44, 1407-1410.
22. Hofmann, M., Campbell, S. J., Ehrhardt, H., Feyerherm, R., "The magnetic behaviour of nanostructured zinc ferrite", J. Mater. Sci., 2004, 39, 5057-5065.
23. Bean, C. P. and Livingston, J. D., "Superparamagnetism", J. Appl. Phys., 1959, 30, 120S-129S.
24. Li, S., Lin, Y. H., Zhang, B. P., Wang, Y., Nan, C. W., "Controlled Fabrication of $BiFeO_3$ Uniform Microcrystals and Their Magnetic and Photocatalytic Behaviors", J. Phys. Chem. C, 2010, 114, 2903-2908.
25. Kislov, N., Srinivasan, S. S., Emirov, Y., Stefanakos, E. K., "Optical absorption red and blue shifts in $ZnFe_2O_4$ nanoparticles", Mater. Sci. Eng. B, 2008, 153, 70-77.
26. Lv, H., Ma, L., Zeng, P., Ke, D., Peng, T., "Synthesis of floriated $ZnFe_2O_4$ with porous nanorod structures and its photocatalytic hydrogen production under visible light", J. Mater. Chem., 2010, 20, 3665-3672.
27. Brus, L. E., "Electron–electron and electron-hole interactions in small semiconductor crystallites: The size dependence of the lowest excited electronic state", J. Chem. Phys., 1984, 80, 4404-4409.

[Downloaded from herasat.iust.ac.ir on 2025-07-19]

[DOI: 10.22068/ijmse.14.1.5]